# Passivity-Based Wind Estimation Using Aircraft

Jeremy W. Hopwood* and Craig A. Woolsey†

Virginia Tech, Blacksburg, VA 24061

April 13, 2023

**Abstract**

This paper presents the development and simulation of a global nonlinear passivity-based observer for aircraft in wind. Wind estimates are vital to the expansion of urban air mobility operations by contributing to model-based atmospheric predictions as well as vehicle-level systems for improved weather tolerance and safety. Traditional approaches to wind estimation rely on linearization of the flight dynamics and thus are only valid near a nominal flight condition. For operations across the flight envelope in a wide variety of wind conditions, a more global result must be obtained. This paper specializes existing passivity-based observer theory to aircraft in wind. The main results of this paper give explicit formulas for necessary gains as well as a linear matrix inequality that can be used to optimize wind estimate convergence. The developed wind observer is implemented on simulation data and shows good performance even when assumptions are violated, indicating its robustness.

## 1 Introduction

Weather patterns over complex terrain are complicated and ever-changing, yet are crucially important to understand for safe air mobility operations [1]. The importance of accurate, real-time weather prediction only increases as NASA's Advanced Air Mobility (AAM) and Urban Air Mobility (UAM) mission concepts mature to bring ubiquity, safety, and efficiency to highly automated air transportation of people and goods in urban and suburban areas [2]. As we mature towards ubiquitous air mobility operations the need grows for higher weather tolerance and thus relaxed margins for flight safety [3, 4, 5, 6]. The expansion of weather-tolerant operations will not just be made possible through more accurate model-based atmospheric predictions on the mesoscale and microscale, but also improved atmospheric measurements at the vehicle level. In particular, the latter can contribute to the former using in situ measurements of wind as illustrated in Figure 1.

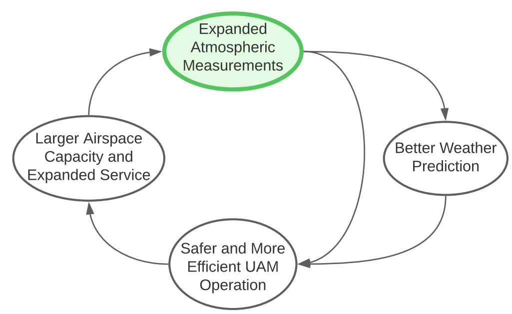


Figure 1: Enabling Air Mobility

Traditional sampling methods such as weather balloons are impractical in an urban setting and only capture a few data points in the atmospheric boundary layer. One of the fastest-emerging solutions to bring higher temporal and spatial resolution to atmospheric measurements is the use of small unmanned aircraft systems (UAS) [7, 8, 9, 10, 11]. The use of UAS enables better atmospheric boundary layer (ABL) profiling and microscale numerical weather prediction (NWP) using high-rate in situ measurements. Of particular interest are approaches that do not require specialized sensors, such as an anemometer to measure wind velocity. The dynamics of the aircraft itself in response to external disturbances can be used to continuously estimate the wind at the aircraft's location. The low instrumentation barrier for implementation makes UAS-based wind estimation an extremely viable and feasible solution for UAS as well as advanced air mobility, package delivery, and emergency services aircraft. This opportunity for crowdsourced sensing provides an extremely rich data set that can be used across disciplines and applications to enable safer, more efficient, and weather-tolerant air mobility operations [12, 13].



*Ph.D. Candidate, Kevin T. Crofton Department of Aerospace and Ocean Engineering, jeremyhopwood@vt.edu

†Professor, Kevin T. Crofton Department of Aerospace and Ocean Engineering, cwoolsey@vt.edu

While the incorporation of weather sensing on air mobility vehicles presents a great opportunity, there are concerns that current approaches would not enable access to regions where data may be needed most, such as areas subject to high winds. Most approaches to aircraft wind estimation rely on a linear flight dynamic modeling approach assuming small perturbations from a nominal flight condition. While these methods work well close to the designed operating condition, the underlying assumptions can be violated in the presence of strong wind. These concerns present a need to expand the range of flight conditions for which accurate wind estimates and atmospheric measurements can be made.

To improve capability to predict weather in an urban environment, this paper presents the design and simulation of a global nonlinear passivity-based wind observer for aircraft. This observer provides real-time estimates of the wind valid across the entire flight envelope. Such an observer creates a capability to expand the range of flight conditions for which accurate wind estimates can be made. One of the main benefits of this nonlinear observer is that it comes with rigorous guarantees on the wind estimate convergence, thus increasing the level of trust in whatever autonomous mission it may be employed. This is where traditional linear approaches and linearization-based approaches such as the extended Kalman filter can come up short. Furthermore, Kalman filtering approaches to wind estimation tend to be very sensitive to assumptions about the statistics of the wind disturbance, which is only exacerbated for flight across a wide variety of conditions.

This paper is organized as follows. Section 2 introduces the aircraft in question and derives the equations of motion in wind for which the observer is designed. Section 3 provides an overview of the theory of passivity-based observers as presented in [14, 15]. The main result of this paper is detailed in Section 4 where the passivity-based observer for aircraft in wind is designed. Section 5 presents simulation results for this observer and evaluates its performance as assumptions are violated. Section 6 states the conclusions of this work along with future research.

## 2 Aircraft Dynamics in Wind

### Rigid-Body Dynamics

Consider an aircraft, modeled as a rigid body of mass $m$. Let unit vectors $\{\boldsymbol{i}_1, \boldsymbol{i}_2, \boldsymbol{i}_3\}$ define an earth-fixed, inertial North-East-Down (NED) orthonormal reference frame, $\mathcal{F}_\mathrm{I}$. Let the unit vectors $\{\boldsymbol{b}_1, \boldsymbol{b}_2, \boldsymbol{b}_3\}$ define the orthonormal body-fixed frame, $\mathcal{F}_\mathrm{B}$, centered at the aircraft center of gravity (CG) with $\boldsymbol{b}_1$ out the front of the aircraft, $\boldsymbol{b}_2$ out of the right-hand side, and $\boldsymbol{b}_3$ out of the bottom completing the right-hand rule. The position of the body frame with respect to the inertial frame is given by the vector $\boldsymbol{q} = [x\ y\ z]^\mathsf{T}$. The attitude of the aircraft is given by the rotation matrix, $\boldsymbol{R}_\mathrm{IB}$, that maps free vectors from $\mathcal{F}_\mathrm{B}$ to $\mathcal{F}_\mathrm{I}$. Consider the Euler angle parameterization

$$\boldsymbol{R}_\mathrm{IB} = e^{\boldsymbol{S}(\boldsymbol{e}_3)\psi} e^{\boldsymbol{S}(\boldsymbol{e}_2)\theta} e^{\boldsymbol{S}(\boldsymbol{e}_1)\phi}$$

where $\phi$, $\theta$, and $\psi$ are the roll, pitch, and yaw angles of the aircraft, respectively. Here, $\boldsymbol{e}_1 = [1\ 0\ 0]^\mathsf{T}$, etc., and $\boldsymbol{S}(\cdot)$ is the skew-symmetric cross product equivalent matrix satisfying $\boldsymbol{S}(\boldsymbol{a})\boldsymbol{b} = \boldsymbol{a}\times\boldsymbol{b}$. Let $\boldsymbol{v} = [u\ v\ w]^\mathsf{T}$ and $\boldsymbol{\omega} = [p\ q\ r]^\mathsf{T}$ be the translational and rotational velocity of the aircraft with respect to $\mathcal{F}_\mathrm{I}$ expressed in $\mathcal{F}_\mathrm{B}$, respectively. Thus, we have the kinematic equations

$$\dot{\boldsymbol{q}} = \boldsymbol{R}_\mathrm{IB}\boldsymbol{v} \tag{1a}$$

$$\dot{\boldsymbol{R}}_\mathrm{IB} = \boldsymbol{R}_\mathrm{IB}\boldsymbol{S}(\boldsymbol{\omega}) \tag{1b}$$

With $\boldsymbol{\Theta} := [\phi\ \theta\ \psi]^\mathsf{T}$, Eq. (1b) becomes

$$\dot{\boldsymbol{\Theta}} = \underbrace{\begin{bmatrix} 1 & \sin\phi\tan\theta & \cos\phi\tan\theta \\ 0 & \cos\phi & -\sin\phi \\ 0 & \sin\phi\sec\theta & \cos\phi\sec\theta \end{bmatrix}}_{\boldsymbol{L}_\mathrm{IB}} \underbrace{\begin{bmatrix} p \\ q \\ r \end{bmatrix}}_{\boldsymbol{\omega}} \tag{2}$$

Alternatively, we may parameterize the attitude of the aircraft using the heading vector, $\boldsymbol{\lambda} = \boldsymbol{R}_\mathrm{IB}^\mathsf{T}\boldsymbol{e}_1$, and tilt vector, $\boldsymbol{\zeta} = \boldsymbol{R}_\mathrm{IB}^\mathsf{T}\boldsymbol{e}_3$, as done in [16, 17, 18, 19]. Then, the the attitude kinematics become

$$\dot{\boldsymbol{\lambda}} = \boldsymbol{\lambda}\times\boldsymbol{\omega}, \quad \dot{\boldsymbol{\zeta}} = \boldsymbol{\zeta}\times\boldsymbol{\omega} \tag{3}$$

where the rotation matrix, $\boldsymbol{R}_\mathrm{IB}$, may be reconstructed as

$$\boldsymbol{R}_\mathrm{IB}(\boldsymbol{\lambda},\boldsymbol{\zeta}) = \begin{bmatrix}\boldsymbol{\lambda} & \boldsymbol{S}(\boldsymbol{\zeta})\boldsymbol{\lambda} & \boldsymbol{\zeta}\end{bmatrix}^\mathsf{T} \tag{4}$$

Let us represent the aerodynamic forces and moments on the aircraft expressed in $\mathcal{F}_\mathrm{B}$ as $\boldsymbol{F}$ and $\boldsymbol{M}$. Define $\boldsymbol{p} = m\boldsymbol{v}$ to be the linear momentum of the aircraft and $\boldsymbol{h} = \boldsymbol{I}\boldsymbol{\omega}$ to be the angular momentum vector about the center of mass, both expressed in $\mathcal{F}_\mathrm{B}$. Here, $\boldsymbol{I}$ is the moment of inertia matrix about the center of mass in $\mathcal{F}_\mathrm{B}$. Altogether, the equations of motion in still air are

$$\dot{\boldsymbol{q}} = \boldsymbol{R}_\mathrm{IB}(\boldsymbol{\lambda},\boldsymbol{\zeta})\boldsymbol{v} \tag{5a}$$

$$\dot{\boldsymbol{\lambda}} = \boldsymbol{\lambda}\times\boldsymbol{\omega} \tag{5b}$$

$$\dot{\boldsymbol{\zeta}} = \boldsymbol{\zeta}\times\boldsymbol{\omega} \tag{5c}$$

$$\dot{\boldsymbol{p}} = \boldsymbol{p}\times\boldsymbol{\omega} + mg\boldsymbol{\zeta} + \boldsymbol{F} \tag{5d}$$

$$\dot{\boldsymbol{h}} = \boldsymbol{h}\times\boldsymbol{\omega} + \boldsymbol{M} \tag{5e}$$

## Dynamics in a Wind Field

Consider the aircraft's motion in wind. In general and independent of the aircraft's motion, the wind is a time-varying vector field, $\boldsymbol{W} : \mathbb{R}^3 \times \mathbb{R} \to \mathbb{R}^3$, defined in the inertial frame. Let the instantaneous wind vector as experienced by the aircraft be

$$\boldsymbol{w}(t) = \boldsymbol{W}(\boldsymbol{q}(t), t) \tag{6}$$

The *apparent wind*, $\boldsymbol{w}$, is part of the aircraft state vector, defined by evaluating the wind field, $\boldsymbol{W}$, at the aircraft's position, $\boldsymbol{q}$, at time $t$. Using the chain rule, the time derivative of $\boldsymbol{w}$ is

$$\frac{\mathrm{d}\boldsymbol{w}}{\mathrm{d}t} = \frac{\partial \boldsymbol{W}}{\partial t}(\boldsymbol{q}, t) + \nabla_q \boldsymbol{W}(\boldsymbol{q}, t)\frac{\mathrm{d}\boldsymbol{q}}{\mathrm{d}t} \tag{7}$$

in agreement with [11]. Note the we have arrived at Eq. (7) under the implicit assumption that the vehicle does not affect the flow field in which it is immersed.

As done by Etkin [20], we may define the angular velocity of the wind as experienced by the aircraft in the body frame, $\boldsymbol{\omega}_\mathrm{w} = \begin{bmatrix} p_\mathrm{w} & q_\mathrm{w} & r_\mathrm{w} \end{bmatrix}^\top$, such that

$$\boldsymbol{\Phi} := \boldsymbol{R}_\mathrm{IB}^\top \nabla_{\boldsymbol{q}} \boldsymbol{W} \boldsymbol{R}_\mathrm{IB} =: \begin{bmatrix} 0 & 0 & 0 \\ r_\mathrm{w} & 0 & 0 \\ -q_\mathrm{w} & p_\mathrm{w} & 0 \end{bmatrix} \tag{8}$$

The matrix $\boldsymbol{\Phi}$ is the local wind gradient matrix expressed in the body frame. In terms of $\boldsymbol{\Phi}$, (7) becomes

$$\dot{\boldsymbol{w}} = \frac{\partial \boldsymbol{W}}{\partial t} + \boldsymbol{R}_\mathrm{IB}\boldsymbol{\Phi}\boldsymbol{v} \tag{9}$$

where $\frac{\partial \boldsymbol{W}}{\partial t}$ is a function of $\boldsymbol{q}$ and $t$.

We now consider the time derivative of the wind gradient as experienced by the aircraft. The goal is a closed-form expression for $\dot{\boldsymbol{\omega}}_w$. However, taking the time derivative of Eq. (8), requires computation of the time derivative of $\nabla_{\boldsymbol{q}}\boldsymbol{W}$. In general, this requires information about (or estimation of) the gradient of the tensor field $\nabla_{\boldsymbol{q}}\boldsymbol{W}$. To simplify the problem, we make the following assumption in order to eliminate the dependence of $\boldsymbol{\omega}_\mathrm{w}$ on vehicle position.

**Assumption 1.** *The change in gradient of the apparent wind on the scale of the aircraft due to its translation through the wind field is sufficiently slow. In other words, $\nabla_{\boldsymbol{q}}\boldsymbol{W}$ is constant.*

Taking the derivative of $\boldsymbol{\omega}_\mathrm{w}$ as defined in Eq. (8) using the chain rule with (2), we obtain

$$\dot{\boldsymbol{\omega}}_w = \frac{\partial \boldsymbol{\omega}_\mathrm{w}}{\partial \boldsymbol{\Theta}} \boldsymbol{L}_\mathrm{IB}\boldsymbol{\omega}\bigg|_{\nabla_{\boldsymbol{q}}\boldsymbol{W} = \boldsymbol{R}_\mathrm{IB}\boldsymbol{\Phi}\boldsymbol{R}_\mathrm{IB}^\top} \tag{10}$$

While this expression looks quite complicated, it simplifies to

$$\dot{\boldsymbol{\omega}}_w = \begin{bmatrix} q_\mathrm{w} r \\ r_\mathrm{w} p - p_\mathrm{w} r \\ -q_\mathrm{w} p \end{bmatrix} \tag{11}$$

We make the assumption the aerodynamic forces and moments only depend on the air mass relative velocity. Therefore, $\boldsymbol{F} = \boldsymbol{F}(\boldsymbol{v}_r, \boldsymbol{\omega}_r, \boldsymbol{u})$ and $\boldsymbol{M} = \boldsymbol{M}(\boldsymbol{v}_r, \boldsymbol{\omega}_r, \boldsymbol{u})$, where $\boldsymbol{u}$ are the aircraft control inputs and

$$\boldsymbol{v}_r = \boldsymbol{v} - \boldsymbol{R}_\mathrm{IB}^\top \boldsymbol{w} \tag{12}$$

$$\boldsymbol{\omega}_r = \boldsymbol{\omega} - \boldsymbol{\omega}_\mathrm{w} \tag{13}$$

Taking the time derivative of Eq. (12), we have

$$\begin{aligned} \dot{\boldsymbol{v}}_r = \boldsymbol{v}_r \times \boldsymbol{\omega} + g\boldsymbol{R}_\mathrm{IB}^\top \boldsymbol{e}_3 + \frac{1}{m}\boldsymbol{F}(\boldsymbol{v}_r, \boldsymbol{\omega}_r, \boldsymbol{u}) \\ - \boldsymbol{R}_\mathrm{IB}^\top \frac{\partial \boldsymbol{W}}{\partial t} - \boldsymbol{\Phi}(\boldsymbol{v}_r + \boldsymbol{R}_\mathrm{IB}^\top \boldsymbol{w}) \end{aligned} \tag{14}$$

Here we have chosen to use variables $\boldsymbol{v}_r$ and $\boldsymbol{w}$, but any other combination of the wind triangle Eq. (12) is equally valid. Unlike the translational velocity, we choose the angular velocity states $\boldsymbol{\omega}$ and $\boldsymbol{\omega}_\mathrm{w}$ because typically $\boldsymbol{\omega}$ is directly measurable. From Eq. (5), the angular velocity dynamics are

$$\dot{\boldsymbol{\omega}} = \boldsymbol{I}^{-1}\left(\boldsymbol{I}\boldsymbol{\omega} \times \boldsymbol{\omega} + \boldsymbol{M}(\boldsymbol{v}_r, \boldsymbol{\omega}_r, \boldsymbol{u})\right) \tag{15}$$

Altogether, the equations of motion of an aircraft in a wind field are

$$\dot{\boldsymbol{q}} = \boldsymbol{R}_\mathrm{IB}\boldsymbol{v}_r + \boldsymbol{w} \tag{16a}$$

$$\dot{\boldsymbol{\lambda}} = \boldsymbol{\lambda} \times \boldsymbol{\omega} \tag{16b}$$

$$\dot{\boldsymbol{\zeta}} = \boldsymbol{\zeta} \times \boldsymbol{\omega} \tag{16c}$$

$$\begin{aligned} \dot{\boldsymbol{v}}_r = \boldsymbol{v}_r \times \boldsymbol{\omega} + g\boldsymbol{\zeta} + \frac{1}{m}\boldsymbol{F}(\boldsymbol{v}_r, \boldsymbol{\omega}_r, \boldsymbol{u}) \\ - \boldsymbol{R}_\mathrm{IB}^\top \frac{\partial \boldsymbol{w}}{\partial t} - \boldsymbol{\Phi}(\boldsymbol{v}_r + \boldsymbol{R}_\mathrm{IB}^\top \boldsymbol{w}) \end{aligned} \tag{16d}$$

$$\dot{\boldsymbol{w}} = \frac{\partial \boldsymbol{W}}{\partial t} + \boldsymbol{R}_\mathrm{IB}\boldsymbol{\Phi}\left(\boldsymbol{v}_r + \boldsymbol{R}_\mathrm{IB}^\top \boldsymbol{w}\right) \tag{16e}$$

$$\dot{\boldsymbol{\omega}} = \boldsymbol{I}^{-1}\left(\boldsymbol{I}\boldsymbol{\omega} \times \boldsymbol{\omega} + \boldsymbol{M}(\boldsymbol{v}_r, \boldsymbol{\omega}_r, \boldsymbol{u})\right) \tag{16f}$$

$$\dot{\boldsymbol{\omega}}_w = \frac{\partial \boldsymbol{\omega}_\mathrm{w}}{\partial \boldsymbol{\Theta}} \boldsymbol{L}_\mathrm{IB}\boldsymbol{\omega}\bigg|_{\nabla_{\boldsymbol{q}}\boldsymbol{W} = \boldsymbol{R}_\mathrm{IB}\boldsymbol{\Phi}\boldsymbol{R}_\mathrm{IB}^\top} \tag{16g}$$

## Simplified Dynamics for Passivity-Based Observer Design

In order to simplify the nonlinear observer design, consider the following two assumptions.

**Assumption 2.** *The wind field is frozen with negligible gradient such that $\dot{\boldsymbol{w}} = \boldsymbol{0}$ and $\boldsymbol{\omega}_\mathrm{w} \equiv \boldsymbol{0}$.*

**Assumption 3.** *For the purpose of estimation, the aircraft's aerodynamics evolve on a time scale significantly slower than the observer dynamics such that at any point in time, the aerodynamics may be taken to be linear, quasi-steady with*

$$\boldsymbol{F} = \boldsymbol{F}_0 + \boldsymbol{F}_v \boldsymbol{v}_r + \boldsymbol{F}_\omega \boldsymbol{\omega} + \boldsymbol{F}_u \boldsymbol{u} \tag{17a}$$

$$\boldsymbol{M} = \boldsymbol{M}_0 + \boldsymbol{M}_v \boldsymbol{v}_r + \boldsymbol{M}_\omega \boldsymbol{\omega} + \boldsymbol{M}_u \boldsymbol{u} \tag{17b}$$

The effect of Assumption 3 is that the quantities $\boldsymbol{F}_{(\cdot)}$ and $\boldsymbol{M}_{(\cdot)}$ are treated as slowly-varying parameters. For example, the values of $\boldsymbol{F}_{(\cdot)}$ and $\boldsymbol{M}_{(\cdot)}$ generally depend on dynamic pressure, $\frac{1}{2}\rho \boldsymbol{v}_r^\top \boldsymbol{v}_r$, which can be assumed to vary sufficiently slowly compared to the observer dynamics. Thus, the plant dynamics for which we want to design a nonlinear observer are

$$\dot{\boldsymbol{q}} = \boldsymbol{R}_{\text{IB}} \boldsymbol{v}_r + \boldsymbol{w} \tag{18a}$$

$$\dot{\boldsymbol{\lambda}} = \boldsymbol{\lambda} \times \boldsymbol{\omega} \tag{18b}$$

$$\dot{\boldsymbol{\zeta}} = \boldsymbol{\zeta} \times \boldsymbol{\omega} \tag{18c}$$

$$\dot{\boldsymbol{\omega}} = \boldsymbol{I}^{-1}\big(\boldsymbol{I}\boldsymbol{\omega} \times \boldsymbol{\omega} + \boldsymbol{M}\big) \tag{18d}$$

$$\dot{\boldsymbol{v}}_r = \boldsymbol{v}_r \times \boldsymbol{\omega} + g\boldsymbol{\zeta} + \frac{1}{m}\boldsymbol{F} \tag{18e}$$

$$\dot{\boldsymbol{w}} = \boldsymbol{0} \tag{18f}$$

with $\boldsymbol{F}$ and $\boldsymbol{M}$ given by Eq. (17). The state of this system is defined by the vector $\boldsymbol{x} = [\boldsymbol{q}^\top\ \boldsymbol{\lambda}^\top\ \boldsymbol{\zeta}^\top\ \boldsymbol{\omega}^\top\ \boldsymbol{v}_r^\top\ \boldsymbol{w}^\top]^\top \in \mathcal{X} \subset \mathbb{R}^n$ where the input vector, $\boldsymbol{u} \in \mathcal{U} \subset \mathbb{R}^m$, is known.

It is often the case that aircraft are instrumented with an accelerometer, gyroscope, magnetometer, and inertial positioning system (i.e. vision-based or GNSS) such that position, attitude, and angular velocity measurements can be readily obtained without noise from a low-level estimation algorithm. Thus, we make the following assumption.

**Assumption 4.** *The aircraft position, attitude, and angular velocity are measured without noise.*

Therefore, let $\boldsymbol{y} = \boldsymbol{x}_1 := [\boldsymbol{q}^\top\ \boldsymbol{\lambda}^\top\ \boldsymbol{\zeta}^\top\ \boldsymbol{\omega}^\top]^\top$. With $\boldsymbol{x} = [\boldsymbol{x}_1^\top\ \boldsymbol{x}_2^\top]^\top$ where $\boldsymbol{x}_2 = [\boldsymbol{v}_r^\top\ \boldsymbol{w}^\top]^\top$, the dynamics are written as

$$\dot{\boldsymbol{x}}_1 = \boldsymbol{f}_1(\boldsymbol{x}_1, \boldsymbol{x}_2, \boldsymbol{u}) \tag{19a}$$

$$\dot{\boldsymbol{x}}_2 = \boldsymbol{f}_2(\boldsymbol{x}_1, \boldsymbol{x}_2, \boldsymbol{u}) \tag{19b}$$

## 3 Passivity-Based Observers

In this paper, we use the passivity-based observer as described in [14]. This approach aims to find an injection gain matrix $\boldsymbol{L}$ and output-feedback law $\boldsymbol{v}$ that render the observer error dynamics strictly passive. First, we recall a dynamical system $\dot{\boldsymbol{x}} = \boldsymbol{f}(\boldsymbol{x}) + \boldsymbol{g}(\boldsymbol{x})\boldsymbol{u}$ with output $\boldsymbol{y} = \boldsymbol{h}(\boldsymbol{x})$ is *dissipative* with respect to the *supply rate* $w(\boldsymbol{u}, \boldsymbol{y})$ if there exists a non-negative smooth *storage function* $W(\boldsymbol{x})$ such that

$$W(\boldsymbol{x}(t)) - W(\boldsymbol{x}(0)) \le \int_0^t w(\boldsymbol{u}(\tau), \boldsymbol{y}(\tau))\, \mathrm{d}\tau \tag{20}$$

The system is considered *passive* if it is dissipative with respect to the supply rate $w(\boldsymbol{u}, \boldsymbol{y}) = \boldsymbol{u}^\top \boldsymbol{y}$. It is *strictly passive* if there also exists a positive definite function $\phi$ such that the system is dissipative with respect to $w(\boldsymbol{u}, \boldsymbol{y}) = \boldsymbol{u}^\top \boldsymbol{y} - \phi$. Passive systems exhibit many desirable properties. Primarily, pure negative output feedback of a zero-state detectable, passive system asymptotically stabilizes the origin. This property among others are described in the seminal work of [21], where the authors also develop the conditions under which a system can be rendered passive by state feedback. Then in [22], these conditions were extended to output-feedback passivation. This is the case for an observer where only some of the states are available for feedback, thus leading to the passivity-based observer design in [15, 14].

We now present an overview of passivity-based observer design as detailed in [14]. Consider the Luenberger-like observer

$$\dot{\hat{\boldsymbol{x}}}_1 = \boldsymbol{f}_1(\hat{\boldsymbol{x}}_1, \hat{\boldsymbol{x}}_2, \boldsymbol{u}) + \boldsymbol{L}_1 \boldsymbol{v}(\hat{\boldsymbol{x}}, \boldsymbol{y}, \boldsymbol{u}) \tag{21a}$$

$$\dot{\hat{\boldsymbol{x}}}_2 = \boldsymbol{f}_2(\hat{\boldsymbol{x}}_1, \hat{\boldsymbol{x}}_2, \boldsymbol{u}) + \boldsymbol{L}_2(\boldsymbol{y}) \boldsymbol{v}(\hat{\boldsymbol{x}}, \boldsymbol{y}, \boldsymbol{u}) \tag{21b}$$

with feedback

$$\boldsymbol{v}(\hat{\boldsymbol{x}}, \boldsymbol{y}, \boldsymbol{u}) = -k(\hat{\boldsymbol{x}}, \boldsymbol{y}, \boldsymbol{u}) \boldsymbol{y}_d + \boldsymbol{v}_d \tag{22}$$

where $\boldsymbol{y}_d = \hat{\boldsymbol{x}}_1 - \boldsymbol{x}_1$ is the desired output and $\boldsymbol{v}_d$ is a dummy input. Note we allow the matrix $\boldsymbol{L}_2$ to depend on measurements like in [23, 24, 25], which is not explicitly considered in [14]; however, the proof does not strictly rely on $\boldsymbol{L}_2$ being constant. Define the estimate error as $\tilde{\boldsymbol{x}} := \hat{\boldsymbol{x}} - \boldsymbol{x}$ and consider the notation $\boldsymbol{F}(\tilde{\boldsymbol{x}}; \boldsymbol{x}; \boldsymbol{u}) := \boldsymbol{f}(\tilde{\boldsymbol{x}} + \boldsymbol{x}, \boldsymbol{u}) - \boldsymbol{f}(\boldsymbol{x}, \boldsymbol{u})$. Then, the state estimate error dynamics are

$$\dot{\tilde{\boldsymbol{x}}}_1 = \boldsymbol{F}_1(\tilde{\boldsymbol{x}}_1, \tilde{\boldsymbol{x}}_2; \boldsymbol{x}_1, \boldsymbol{x}_2; \boldsymbol{u}) + \boldsymbol{L}_1 \boldsymbol{v}(\hat{\boldsymbol{x}}, \boldsymbol{y}, \boldsymbol{u}) \tag{23a}$$

$$\dot{\tilde{\boldsymbol{x}}}_2 = \boldsymbol{F}_2(\tilde{\boldsymbol{x}}_1, \tilde{\boldsymbol{x}}_2; \boldsymbol{x}_1, \boldsymbol{x}_2; \boldsymbol{u}) + \boldsymbol{L}_2(\boldsymbol{y}) \boldsymbol{v}(\hat{\boldsymbol{x}}, \boldsymbol{y}, \boldsymbol{u}) \tag{23b}$$

The observer design involves two main steps. First, with $\boldsymbol{y}_d$ viewed as the output, we find a proper Lyapunov function $V^*(\tilde{\boldsymbol{x}}_2, \boldsymbol{x})$ and a positive definite function $\psi_3$ that prove the *augmented system* composed of the error dynamics in Eq. (23) and the plant dynamics is globally minimum phase with respect to the manifold

$$\mathcal{M} = \{(\tilde{\boldsymbol{x}}, \boldsymbol{x}) \mid \tilde{\boldsymbol{x}} = \boldsymbol{0}\} \tag{24}$$

with $\dot{V}^* \leq -\psi_3(\|\tilde{\boldsymbol{x}}_2\|)$. This step can be thought of like the first step in integrator backstepping, where one stabilizes a subsystem with no available inputs [26]. Here, we ensure the unmeasured state estimates asymptotically approach their true values when the measurable states are known. Second, we find nonnegative functions $\varphi_1$ and $\varphi_2$ such that

$$\begin{aligned}\Bigg| &\frac{\partial V^*}{\partial \tilde{\boldsymbol{x}}_2}[\boldsymbol{F}_2 - \boldsymbol{L}_2\boldsymbol{L}_1^{-1}\boldsymbol{F}_1](\tilde{\boldsymbol{x}}_1, \boldsymbol{L}_2\boldsymbol{L}_1^{-1}\tilde{\boldsymbol{x}}_1; \boldsymbol{x}_1, \hat{\boldsymbol{x}}_2; \boldsymbol{u}) \\ &+ \tilde{\boldsymbol{x}}_1\boldsymbol{L}_1^{-1}\boldsymbol{F}_1(\tilde{\boldsymbol{x}}_1, \tilde{\boldsymbol{x}}_2 + \boldsymbol{L}_2\boldsymbol{L}_1^{-1}\tilde{\boldsymbol{x}}_1; \boldsymbol{x}_1, \hat{\boldsymbol{x}}_2 - \tilde{\boldsymbol{x}}_2; \boldsymbol{u})\Bigg| \\ &\leq \varphi_1(\tilde{\boldsymbol{x}}_1, \boldsymbol{x}_1, \hat{\boldsymbol{x}}_2, \boldsymbol{u})\|\tilde{\boldsymbol{x}}_1\|^2 \\ &+ \varphi_2(\tilde{\boldsymbol{x}}_1, \boldsymbol{x}_1, \hat{\boldsymbol{x}}_2, \boldsymbol{u})\psi_3^{1/2}(\|\tilde{\boldsymbol{x}}_2\|)\|\tilde{\boldsymbol{x}}_1\| \end{aligned} \tag{25}$$

In this expression, parentheses contain arguments for all functions in square brackets. The requirement that there exists these *bounding functions* comes from the sufficient conditions for output feedback passivation developed in [22]. It essentially ensures the coupling between the output dynamics ($\dot{\tilde{\boldsymbol{x}}}_1$) and the unmeasurable dynamics ($\dot{\tilde{\boldsymbol{x}}}_2$) preserves strict passivity from $\boldsymbol{v}_d$ to $\boldsymbol{y}_d$, which is a result of the following.

**Theorem 1** (Theorem 2 in [14])**.** *Suppose the Lyapunov function $V^*$ proves the augmented system is (globally) minimum phase with respect to $\mathcal{M}$. Also suppose there exists $\varphi_1$ and $\varphi_2$ such that Eq. (25) holds. Then, the feedback*

$$\boldsymbol{v} = -k(\hat{\boldsymbol{x}}, \boldsymbol{y})\boldsymbol{y}_d + \boldsymbol{v}_d \tag{26}$$

*with*

$$\begin{aligned}k(\hat{\boldsymbol{x}}, \boldsymbol{y}) &= \varepsilon + \varphi_1(\hat{\boldsymbol{x}}_1 - \boldsymbol{y}, \boldsymbol{y}, \hat{\boldsymbol{x}}_2 - \boldsymbol{L}_2\boldsymbol{L}_1^{-1}(\hat{\boldsymbol{x}}_1 - \boldsymbol{y})) \\ &+ \varphi_2^2(\hat{\boldsymbol{x}}_1 - \boldsymbol{y}, \boldsymbol{y}, \hat{\boldsymbol{x}}_2 - \boldsymbol{L}_2\boldsymbol{L}_1^{-1}(\hat{\boldsymbol{x}}_1 - \boldsymbol{y})),\ \varepsilon > 0\end{aligned} \tag{27}$$

*renders the augmented system strictly passive from $\boldsymbol{v}_d$ to $\boldsymbol{y}_d$ with respect to $\mathcal{M}$ with the storage function*

$$W = V^*(\tilde{\boldsymbol{x}}_2 - \boldsymbol{L}_2\boldsymbol{L}_1^{-1}\tilde{\boldsymbol{x}}_1, \boldsymbol{x}) + \frac{1}{2}\tilde{\boldsymbol{x}}_1^\intercal\boldsymbol{L}_1^{-1}\tilde{\boldsymbol{x}}_1 \tag{28}$$

*Upon setting $\boldsymbol{v}_d = \boldsymbol{0}$, $\mathcal{M}$ becomes positively invariant and (globally) asymptotically attractive.*

## 4 Passivity-Based Observer Design for Aircraft in Wind

### Minimum Phase and Relative Degree Sufficient Conditions

Now consider the aircraft in wind described by Eq. (18). The components of the error dynamics vector field $\boldsymbol{F}_{(\cdot)}$ as defined in Eq. (23) are

$$\begin{aligned}\boldsymbol{F}_{1_q} &= \boldsymbol{R}_{\mathrm{IB}}(\tilde{\boldsymbol{\lambda}} + \boldsymbol{\lambda}, \tilde{\boldsymbol{\zeta}} + \boldsymbol{\zeta})(\tilde{\boldsymbol{v}}_r + \boldsymbol{v}_r) \\ &\quad - \boldsymbol{R}_{\mathrm{IB}}(\boldsymbol{\lambda}, \boldsymbol{\zeta})\boldsymbol{v}_r + \tilde{\boldsymbol{w}} &\text{(29a)} \\ \boldsymbol{F}_{1_\lambda} &= \boldsymbol{S}(\tilde{\boldsymbol{\lambda}} + \boldsymbol{\lambda})(\tilde{\boldsymbol{\omega}} + \boldsymbol{\omega}) - \boldsymbol{S}(\boldsymbol{\lambda})\boldsymbol{\omega} &\text{(29b)} \\ \boldsymbol{F}_{1_\zeta} &= \boldsymbol{S}(\tilde{\boldsymbol{\zeta}} + \boldsymbol{\zeta})(\tilde{\boldsymbol{\omega}} + \boldsymbol{\omega}) - \boldsymbol{S}(\boldsymbol{\zeta})\boldsymbol{\omega} &\text{(29c)} \\ \boldsymbol{F}_{1_\omega} &= \boldsymbol{I}^{-1}\big(\boldsymbol{S}(\boldsymbol{I}\tilde{\boldsymbol{\omega}} + \boldsymbol{I}\boldsymbol{\omega})(\tilde{\boldsymbol{\omega}} + \boldsymbol{\omega}) - \boldsymbol{S}(\boldsymbol{I}\boldsymbol{\omega})\boldsymbol{\omega} \\ &\quad + \boldsymbol{M}_v\tilde{\boldsymbol{v}}_r + \boldsymbol{M}_\omega\tilde{\boldsymbol{\omega}}\big) &\text{(29d)} \\ \boldsymbol{F}_{2_{v_r}} &= \boldsymbol{S}(\tilde{\boldsymbol{v}}_r + \boldsymbol{v}_r)(\tilde{\boldsymbol{\omega}} + \boldsymbol{\omega}) - \boldsymbol{S}(\boldsymbol{v}_r)\boldsymbol{\omega} + g\tilde{\boldsymbol{\zeta}} \\ &\quad + \frac{1}{m}(\boldsymbol{F}_v\tilde{\boldsymbol{v}}_r + \boldsymbol{F}_\omega\tilde{\boldsymbol{\omega}}) &\text{(29e)} \\ \boldsymbol{F}_{2_w} &= \boldsymbol{0} &\text{(29f)}\end{aligned}$$

We now aim to design $\boldsymbol{L}$ such that the first condition in Theorem 1 holds. Considering the feedback injection term in Eq. (26), the zero dynamics of the *augmented system* composed of Eqs. (18) and (29) is analyzed in view of the input-output pair $(\boldsymbol{v}_d, \boldsymbol{y}_d)$. In general, the *zero dynamics* of the augmented system with respect to $\boldsymbol{y}_d$ exist in some neighborhood $\mathcal{Z} \subseteq \mathcal{X} \times \mathcal{X}$ about $\tilde{\boldsymbol{x}} = \boldsymbol{0}$ [21] and evolve on $\mathcal{Z}^* = \{(\tilde{\boldsymbol{x}}, \boldsymbol{x}) \in \mathcal{Z} \mid \tilde{\boldsymbol{x}}_1 \equiv \boldsymbol{0}\}$. As discussed in [14], the zero dynamics can can be shown to satisfy

$$\dot{\tilde{\boldsymbol{x}}}_2 = \left[\boldsymbol{F}_2 - \boldsymbol{L}_2\boldsymbol{L}_1^{-1}\boldsymbol{F}_1\right](\boldsymbol{0}, \tilde{\boldsymbol{x}}_2; \boldsymbol{x}_1, \boldsymbol{x}_2; \boldsymbol{u}) \tag{30}$$

$$\dot{\boldsymbol{x}} = \boldsymbol{f}(\boldsymbol{x}, \boldsymbol{u}) \tag{31}$$

Therefore, we must choose $\boldsymbol{L}$ such that $\tilde{\boldsymbol{x}}_2 = \boldsymbol{0}$ is asymptotically stable on $\mathcal{Z}^*$. Here, we see the global existence of the zero dynamics ($\mathcal{Z} = \mathcal{X} \times \mathcal{X}$) only requires $\boldsymbol{L}_1$ to be invertible, also implying the error dynamics have vector relative degree $\{1, \cdots, 1\}$[22]. For convenience, denote

$$\boldsymbol{E}_2 := \boldsymbol{F}_2 - \boldsymbol{L}_2\boldsymbol{L}_1^{-1}\boldsymbol{F}_1 \tag{32a}$$

$$\implies \boldsymbol{E}_2^* := \boldsymbol{E}_2(\boldsymbol{0}, \tilde{\boldsymbol{x}}_2; \boldsymbol{x}_1, \boldsymbol{x}_2; \boldsymbol{u}) \tag{32b}$$

Then partitioning $\boldsymbol{L}$ as

$$\boldsymbol{L}_1 = \mathbf{diag}\left(\boldsymbol{L}_{1_q}, \boldsymbol{L}_{1_\lambda}, \boldsymbol{L}_{1_\zeta}, \boldsymbol{L}_{1_\omega}\right) \tag{33a}$$

$$\boldsymbol{L}_2 = \begin{bmatrix}\boldsymbol{L}_{2_{v,q}} & \boldsymbol{L}_{2_{v,\lambda}} & \boldsymbol{L}_{2_{v,\zeta}} & \boldsymbol{L}_{2_{v,\omega}} \\ \boldsymbol{L}_{2_{w,q}} & \boldsymbol{L}_{2_{w,\lambda}} & \boldsymbol{L}_{2_{w,\zeta}} & \boldsymbol{L}_{2_{w,\omega}}\end{bmatrix} \tag{33b}$$

we compute $\boldsymbol{E}_{2_{v_r}}$ and $\boldsymbol{E}_{2_w}$ as defined in Eq. (32a). Then, the zero dynamics are obtained by simply evaluating Eq. (32a) at $\boldsymbol{y}_d = \tilde{\boldsymbol{x}}_1 = \boldsymbol{0}$. As a result,

$$\begin{aligned}\boldsymbol{E}_{2_{v_r}}^* &= -\boldsymbol{S}(\boldsymbol{\omega})\tilde{\boldsymbol{v}}_r + \frac{1}{m}\boldsymbol{F}_v\tilde{\boldsymbol{v}}_r - \boldsymbol{L}_{2_{v,\omega}}\boldsymbol{L}_{1_\omega}^{-1}\boldsymbol{I}^{-1}\boldsymbol{M}_v\tilde{\boldsymbol{v}}_r \\ &\quad - \boldsymbol{L}_{2_{v,q}}\boldsymbol{L}_{1_q}^{-1}\left(\boldsymbol{R}_{\mathrm{IB}}(\boldsymbol{\lambda}, \boldsymbol{\zeta})\tilde{\boldsymbol{v}}_r + \tilde{\boldsymbol{w}}\right) &\text{(34a)} \\ \boldsymbol{E}_{2_w}^* &= -\boldsymbol{L}_{2_{w,q}}\boldsymbol{L}_{1_q}^{-1}\left(\boldsymbol{R}_{\mathrm{IB}}(\boldsymbol{\lambda}, \boldsymbol{\zeta})\tilde{\boldsymbol{v}}_r + \tilde{\boldsymbol{w}}\right) \\ &\quad - \boldsymbol{L}_{2_{w,\omega}}\boldsymbol{L}_{1_\omega}^{-1}\boldsymbol{I}^{-1}\boldsymbol{M}_v\tilde{\boldsymbol{v}}_r &\text{(34b)}\end{aligned}$$

Consider the zero-error manifold, $\mathcal{M}$, defined in Eq. (24). We aim to find a proper Lyapunov function $V^*(\tilde{\boldsymbol{x}}_2, \boldsymbol{x})$ that proves $\mathcal{M}$ is positively invariant and globally asymptotically attractive on $\mathcal{Z}^*$. This amounts to the conditions

$$\psi_1(\|\tilde{\boldsymbol{x}}_2\|) \leq V^*(\tilde{\boldsymbol{x}}_2, \boldsymbol{x}) \leq \psi_2(\|\tilde{\boldsymbol{x}}_2\|) \tag{35}$$

$$\dot{V}^* = \frac{\partial V^*}{\partial \tilde{\boldsymbol{x}}_2} \boldsymbol{E}_2^* + \frac{\partial V^*}{\partial \boldsymbol{x}} \boldsymbol{f} \leq -\psi_3(\|\tilde{\boldsymbol{x}}_2\|) \tag{36}$$

where $\psi_1, \psi_2$ are class $\mathcal{K}_\infty$ functions and $\psi_3$ is a smooth, positive definite function. Note that $V^*$ does not necessarily depend on $\boldsymbol{x}$, but allowing it to do so, may admit observer designs for a wider class of systems [14]. Fortunately for the aircraft in question, we need only consider the Lyapunov candidate

$$V^*(\tilde{\boldsymbol{x}}_2, \boldsymbol{x}) = \frac{1}{2} \tilde{\boldsymbol{x}}_2^\top \tilde{\boldsymbol{x}}_2 \tag{37}$$

which clearly satisfies Eq. (35). It follows that

$$\begin{aligned} \dot{V}^* = & -\tilde{\boldsymbol{v}}_r^\top \boldsymbol{S}(\boldsymbol{\omega}) \tilde{\boldsymbol{v}}_r + \tilde{\boldsymbol{v}}_r^\top \frac{1}{m} \boldsymbol{F}_v \tilde{\boldsymbol{v}}_r - \tilde{\boldsymbol{v}}_r^\top \boldsymbol{L}_{2_{v,q}} \boldsymbol{L}_{1_q}^{-1} \tilde{\boldsymbol{w}} \\ & - \tilde{\boldsymbol{v}}_r^\top \boldsymbol{L}_{2_{v,q}} \boldsymbol{L}_{1_q}^{-1} \boldsymbol{R}_{\mathrm{IB}} \tilde{\boldsymbol{v}}_r - \tilde{\boldsymbol{v}}_r^\top \boldsymbol{L}_{2_{v,\omega}} \boldsymbol{L}_{1_\omega}^{-1} \boldsymbol{I}^{-1} \boldsymbol{M}_v \tilde{\boldsymbol{v}}_r \\ & - \tilde{\boldsymbol{w}}^\top \boldsymbol{L}_{2_{w,q}} \boldsymbol{L}_{1_q}^{-1} \boldsymbol{R}_{\mathrm{IB}} \tilde{\boldsymbol{v}}_r - \tilde{\boldsymbol{w}}^\top \boldsymbol{L}_{2_{w,q}} \boldsymbol{L}_{1_q}^{-1} \tilde{\boldsymbol{w}} \\ & - \tilde{\boldsymbol{w}}^\top \boldsymbol{L}_{2_{w,\omega}} \boldsymbol{L}_{1_\omega}^{-1} \boldsymbol{I}^{-1} \boldsymbol{M}_v \tilde{\boldsymbol{v}}_r \end{aligned} \tag{38}$$

Here we have dropped the the argument to $\boldsymbol{R}_{\mathrm{IB}}$ for compactness. From here on, it is implied that be $\boldsymbol{R}_{\mathrm{IB}} = \boldsymbol{R}_{\mathrm{IB}}(\boldsymbol{\lambda}, \boldsymbol{\zeta})$ unless explicitly stated. Notice the term $\tilde{\boldsymbol{v}}_r^\top \boldsymbol{S}(\boldsymbol{\omega}) \tilde{\boldsymbol{v}}_r$ is identically equal to zero since the quadratic form of a skew-symmetric matrix is zero. We may then write Eq. (38) as $\dot{V}^* = -\tilde{\boldsymbol{x}}_2^\top \boldsymbol{P} \tilde{\boldsymbol{x}}_2$, where

$$\begin{aligned} \boldsymbol{P}_{11} = & -\frac{1}{m} \boldsymbol{F}_v + \boldsymbol{L}_{2_{v,q}} \boldsymbol{L}_{1_q}^{-1} \boldsymbol{R}_{\mathrm{IB}} \\ & + \boldsymbol{L}_{2_{v,\omega}} \boldsymbol{L}_{1_\omega}^{-1} \boldsymbol{I}^{-1} \boldsymbol{M}_v \end{aligned} \tag{39a}$$

$$\boldsymbol{P}_{12} = \boldsymbol{L}_{2_{v,q}} \boldsymbol{L}_{1_q}^{-1} \tag{39b}$$

$$\boldsymbol{P}_{21} = \boldsymbol{L}_{2_{w,q}} \boldsymbol{L}_{1_q}^{-1} \boldsymbol{R}_{\mathrm{IB}} + \boldsymbol{L}_{2_{w,\omega}} \boldsymbol{L}_{1_\omega}^{-1} \boldsymbol{I}^{-1} \boldsymbol{M}_v \tag{39c}$$

$$\boldsymbol{P}_{22} = \boldsymbol{L}_{2_{w,q}} \boldsymbol{L}_{1_q}^{-1} \tag{39d}$$

Therefore, we will choose the gain matrix $\boldsymbol{L}$ such that

$$\begin{bmatrix} \boldsymbol{Q}_{11} & \boldsymbol{Q}_{12} \\ \boldsymbol{Q}_{12}^\top & \boldsymbol{Q}_{22} \end{bmatrix} := \boldsymbol{Q} := \frac{1}{2} \left( \boldsymbol{P} + \boldsymbol{P}^\top \right) \succ \boldsymbol{0}$$

which is sufficient for proving $\dot{V}^* \prec \boldsymbol{0}$. Let us choose

$$\boldsymbol{L}_{2_{v,q}} = \boldsymbol{\Gamma}_{v,q} \boldsymbol{R}_{\mathrm{IB}}^\top \boldsymbol{L}_{1_q} \tag{40a}$$

$$\boldsymbol{L}_{2_{v,\omega}} = \boldsymbol{\Gamma}_{v,\omega} \boldsymbol{M}_v^\top \boldsymbol{I} \boldsymbol{L}_{1_\omega} \tag{40b}$$

$$\boldsymbol{L}_{2_{w,q}} = \boldsymbol{R}_{\mathrm{IB}} \boldsymbol{\Gamma}_{w,q} \boldsymbol{R}_{\mathrm{IB}}^\top \boldsymbol{L}_{1_q} \tag{40c}$$

$$\boldsymbol{L}_{2_{w,\omega}} = \boldsymbol{R}_{\mathrm{IB}} \boldsymbol{\Gamma}_{w,\omega} \boldsymbol{M}_v^\top \boldsymbol{I} \boldsymbol{L}_{1_\omega} \tag{40d}$$

where the matrix

$$\boldsymbol{\Gamma} = \begin{bmatrix} \boldsymbol{\Gamma}_{v,q} & \boldsymbol{\Gamma}_{v,\omega} \\ \boldsymbol{\Gamma}_{w,q} & \boldsymbol{\Gamma}_{w,\omega} \end{bmatrix} \tag{41}$$

is a constant parameter used for tuning. Notice we have chosen $\boldsymbol{L}_2$ to make the design of $\boldsymbol{L}_1$ independent of the zero dynamics. Then, $\boldsymbol{Q}$ reduces to

$$\begin{aligned} \boldsymbol{Q}_{11} = & -\frac{1}{2m} \left( \boldsymbol{F}_v + \boldsymbol{F}_v^\top \right) + \frac{1}{2} \left( \boldsymbol{\Gamma}_{v,q} + \boldsymbol{\Gamma}_{v,q}^\top \right) \\ & + \frac{1}{2} \left( \boldsymbol{\Gamma}_{v,\omega} \boldsymbol{M}_v^\top \boldsymbol{M}_v + \boldsymbol{M}_v^\top \boldsymbol{M}_v \boldsymbol{\Gamma}_{v,\omega}^\top \right) \end{aligned} \tag{42a}$$

$$\boldsymbol{Q}_{12} = \frac{1}{2} \left( \boldsymbol{\Gamma}_{v,q} + \boldsymbol{\Gamma}_{w,q}^\top + \boldsymbol{M}_v^\top \boldsymbol{M}_v \boldsymbol{\Gamma}_{w,\omega}^\top \right) \boldsymbol{R}_{\mathrm{IB}}^\top \tag{42b}$$

$$\boldsymbol{Q}_{22} = \frac{1}{2} \boldsymbol{R}_{\mathrm{IB}} \left( \boldsymbol{\Gamma}_{w,q} + \boldsymbol{\Gamma}_{w,q}^\top \right) \boldsymbol{R}_{\mathrm{IB}}^\top \tag{42c}$$

The rotation matrix, $\boldsymbol{R}_{\mathrm{IB}}$, does not influence the definiteness of $\boldsymbol{Q}$. This can be seen using the Schur complement where $\boldsymbol{Q} \succ \boldsymbol{0}$ if and only if

$$\boldsymbol{\Gamma}_{w,q} + \boldsymbol{\Gamma}_{w,q}^\top \succ \boldsymbol{0} \tag{43}$$

and $\boldsymbol{Q}_{11} - \boldsymbol{Q}_{12} \boldsymbol{Q}_{22}^{-1} \boldsymbol{Q}_{12}^\top \succ \boldsymbol{0}$. Therefore, we may choose $\boldsymbol{\Gamma}$ such that

$$\begin{aligned} & \begin{bmatrix} -\frac{1}{m} \boldsymbol{F}_v + \boldsymbol{\Gamma}_{v,q} + \boldsymbol{\Gamma}_{v,\omega} \boldsymbol{M}_v^\top \boldsymbol{M}_v & \boldsymbol{\Gamma}_{v,q} \\ \boldsymbol{\Gamma}_{w,q} + \boldsymbol{\Gamma}_{w,\omega} \boldsymbol{M}_v^\top \boldsymbol{M}_v & \boldsymbol{\Gamma}_{w,q} \end{bmatrix} \\ + & \begin{bmatrix} -\frac{1}{m} \boldsymbol{F}_v + \boldsymbol{\Gamma}_{v,q} + \boldsymbol{\Gamma}_{v,\omega} \boldsymbol{M}_v^\top \boldsymbol{M}_v & \boldsymbol{\Gamma}_{v,q} \\ \boldsymbol{\Gamma}_{w,q} + \boldsymbol{\Gamma}_{w,\omega} \boldsymbol{M}_v^\top \boldsymbol{M}_v & \boldsymbol{\Gamma}_{w,q} \end{bmatrix}^\top \succ \boldsymbol{0} \end{aligned} \tag{44}$$

This condition may be stated in the form of the linear matrix inequality (LMI),

$$\boldsymbol{\Gamma} \mathcal{A} + \mathcal{A}^\top \boldsymbol{\Gamma}^\top + \mathcal{Q} \succeq \gamma \mathbb{I} \tag{45}$$

for some positive $\gamma$ where

$$\mathcal{A} = \begin{bmatrix} \mathbb{I} & \mathbb{I} \\ \boldsymbol{M}_v^\top \boldsymbol{M}_v & \boldsymbol{0} \end{bmatrix}, \quad \mathcal{Q} = \begin{bmatrix} -\frac{1}{m} (\boldsymbol{F}_v + \boldsymbol{F}_v^\top) & \boldsymbol{0} \\ \boldsymbol{0} & \boldsymbol{0} \end{bmatrix} \tag{46}$$

One approach is to maximize $\gamma$ with $\boldsymbol{\Gamma}$ being

$$\underset{\boldsymbol{\Gamma}}{\arg\max}\ \gamma \quad \text{subject to Eqs. (43) and (45)} \tag{47}$$

This convex optimization problem yields the matrix $\boldsymbol{\Gamma}$ that maximizes the convergence rate of the zero dynamics. As seen above, the upper bound on $\gamma$ directly depends on the aircraft mass, $\boldsymbol{F}_v$, and $\boldsymbol{M}_v$. In other words, the dissipation rate of relative velocity and wind observation error is dependent on the aircraft's physical dissipation due to drag. Practically, this means there is an upper limit of the time scale of wind fluctuations that can be accurately resolved. However, it remains a possibility there exists a different Lyapunov function or a different dynamic model for $\boldsymbol{w}$ that removes this limitation.

With $\boldsymbol{\Gamma}$ chosen such that Eq. (45) holds, we see

$$\dot{V}^* = -\tilde{\boldsymbol{x}}_2^\top \boldsymbol{Q} \tilde{\boldsymbol{x}}_2 \leq -\frac{\gamma}{2}\|\tilde{\boldsymbol{x}}_2\|^2 =: -\psi_3(\|\tilde{\boldsymbol{x}}_2\|) \quad (48)$$

thus proving the error system is globally minimum phase with respect to $\boldsymbol{y}_d = \hat{\boldsymbol{x}}_1 - \boldsymbol{x}_1$.

## Bounding Functions and Strict Passivity

Next, we need to satisfy the second condition of Theorem 1 and find continuous, non-negative functions $\varphi_1$ and $\varphi_2$ such that Eq. (25) holds. As will be shown in [27], the left-hand side of Eq. (25) can be written as

$$\Bigg| \frac{\partial V^*}{\partial \tilde{\boldsymbol{x}}_2} \boldsymbol{E}_2(\tilde{\boldsymbol{x}}_1, \boldsymbol{L}_2\boldsymbol{L}_1^{-1}\tilde{\boldsymbol{x}}_1; \boldsymbol{x}_1, \hat{\boldsymbol{x}}_2; \boldsymbol{u}) + \tilde{\boldsymbol{x}}_1 \boldsymbol{L}_1^{-1} \boldsymbol{F}_1(\tilde{\boldsymbol{x}}_1, \tilde{\boldsymbol{x}}_2 + \boldsymbol{L}_2\boldsymbol{L}_1^{-1}\tilde{\boldsymbol{x}}_1; \boldsymbol{x}_1, \hat{\boldsymbol{x}}_2 - \tilde{\boldsymbol{x}}_2; \boldsymbol{u}) \Bigg| = \left|\tilde{\boldsymbol{x}}_2^\top \boldsymbol{B}(\tilde{\boldsymbol{x}}_1, \boldsymbol{x}_1, \hat{\boldsymbol{x}}_2)\tilde{\boldsymbol{x}}_1 + \tilde{\boldsymbol{x}}_1^\top \boldsymbol{A}(\tilde{\boldsymbol{x}}_1, \boldsymbol{x}_1, \hat{\boldsymbol{x}}_2)\tilde{\boldsymbol{x}}_1\right| \quad (49)$$

where $\boldsymbol{A}$ and $\boldsymbol{B}$ are matrix functions of appropriate dimensions. Then by the triangle inequality and a series of sub-multiplicative properties,

$$\begin{aligned} &\left|\tilde{\boldsymbol{x}}_1^\top \boldsymbol{A}(\tilde{\boldsymbol{x}}_1, \boldsymbol{x}_1, \hat{\boldsymbol{x}}_2)\tilde{\boldsymbol{x}}_1 + \tilde{\boldsymbol{x}}_2^\top \boldsymbol{B}(\tilde{\boldsymbol{x}}_1, \boldsymbol{x}_1, \hat{\boldsymbol{x}}_2)\tilde{\boldsymbol{x}}_1\right| \\ &\leq \left|\tilde{\boldsymbol{x}}_1^\top \boldsymbol{A}(\tilde{\boldsymbol{x}}_1, \boldsymbol{x}_1, \hat{\boldsymbol{x}}_2)\tilde{\boldsymbol{x}}_1\right| + \left|\tilde{\boldsymbol{x}}_2^\top \boldsymbol{B}(\tilde{\boldsymbol{x}}_1, \boldsymbol{x}_1, \hat{\boldsymbol{x}}_2)\tilde{\boldsymbol{x}}_1\right| \\ &\leq \|\boldsymbol{A}(\tilde{\boldsymbol{x}}_1, \boldsymbol{x}_1, \hat{\boldsymbol{x}}_2)\|_{\mathcal{F}}\|\tilde{\boldsymbol{x}}_1\|_{\mathcal{F}}^2 \\ &\qquad + \|\boldsymbol{B}(\tilde{\boldsymbol{x}}_1, \boldsymbol{x}_1, \hat{\boldsymbol{x}}_2)\|_{\mathcal{Z}}\|\tilde{\boldsymbol{x}}_2\|_{\mathcal{Z}}\|\tilde{\boldsymbol{x}}_1\|_{\mathcal{Z}} \end{aligned} \quad (50)$$

where $\|\cdot\|_{\mathcal{F}}$ is the Frobenius norm (simplifies to the Euclidean norm for the vector $\tilde{\boldsymbol{x}}_1$), and $\|\cdot\|_{\mathcal{Z}}$ is a generalization of the norm used to prove asymptotic stability of the zero dynamics from Eq. (48). Due to the LMI result, it is simply defined as $\|\boldsymbol{B}\|_{\mathcal{Z}} := \sqrt{\frac{\gamma}{2}}\|\boldsymbol{B}\|_{\mathcal{F}}$, but in general could be more complicated given a different $\psi_3$. For $\boldsymbol{B} = \tilde{\boldsymbol{x}}_2$, the norm $\|\tilde{\boldsymbol{x}}_2\|_{\mathcal{Z}}^2$ is equivalent to $\psi_3(\|\tilde{\boldsymbol{x}}_2\|)$. Therefore,

$$\Bigg| \frac{\partial V^*}{\partial \tilde{\boldsymbol{x}}_2} \boldsymbol{E}_2(\tilde{\boldsymbol{x}}_1, \boldsymbol{L}_2\boldsymbol{L}_1^{-1}\tilde{\boldsymbol{x}}_1; \boldsymbol{x}_1, \hat{\boldsymbol{x}}_2; \boldsymbol{u}) + \tilde{\boldsymbol{x}}_1 \boldsymbol{L}_1^{-1} \boldsymbol{F}_1(\tilde{\boldsymbol{x}}_1, \tilde{\boldsymbol{x}}_2 + \boldsymbol{L}_2\boldsymbol{L}_1^{-1}\tilde{\boldsymbol{x}}_1; \boldsymbol{x}_1, \hat{\boldsymbol{x}}_2 - \tilde{\boldsymbol{x}}_2; \boldsymbol{u}) \Bigg| \leq \|\boldsymbol{A}(\tilde{\boldsymbol{x}}_1, \boldsymbol{x}_1, \hat{\boldsymbol{x}}_2)\|_{\mathcal{F}}\|\tilde{\boldsymbol{x}}_1\|_{\mathcal{F}}^2 + \|\boldsymbol{B}(\tilde{\boldsymbol{x}}_1, \boldsymbol{x}_1, \hat{\boldsymbol{x}}_2)\|_{\mathcal{Z}}\psi_3^{1/2}(\|\tilde{\boldsymbol{x}}_2\|)\|\tilde{\boldsymbol{x}}_1\|_{\mathcal{Z}} \quad (51)$$

and $\varphi_1$ and $\varphi_2$ can be taken to be

$$\varphi_1(\tilde{\boldsymbol{x}}_1, \boldsymbol{x}_1, \hat{\boldsymbol{x}}_2) = \|\boldsymbol{A}(\tilde{\boldsymbol{x}}_1, \boldsymbol{x}_1, \hat{\boldsymbol{x}}_2)\|_{\mathcal{F}} \quad (52)$$
$$\varphi_2(\tilde{\boldsymbol{x}}_1, \boldsymbol{x}_1, \hat{\boldsymbol{x}}_2) = \|\boldsymbol{B}(\tilde{\boldsymbol{x}}_1, \boldsymbol{x}_1, \hat{\boldsymbol{x}}_2)\|_{\mathcal{Z}} \quad (53)$$

satisfying the second condition in Theorem 1.

Note these choices of $\varphi_1$ and $\varphi_2$ hold for any block-diagonal, invertible $\boldsymbol{L}_1$ and any finite $\boldsymbol{L}_{2_{v,\lambda}}$, $\boldsymbol{L}_{2_{v,\zeta}}$, $\boldsymbol{L}_{2_{w,\lambda}}$, $\boldsymbol{L}_{2_{w,\zeta}}$. However, the observer gain is then also arbitrarily large. Therefore, it is judicious to choose these gains to make $\varphi_1$ and $\varphi_2$ as small as possible. It turns out that setting $\boldsymbol{L}_{2_{v,\lambda}}$, $\boldsymbol{L}_{2_{v,\zeta}}$, $\boldsymbol{L}_{2_{w,\lambda}}$, and $\boldsymbol{L}_{2_{w,\zeta}}$ to be zero matrices accomplishes this task. Intuitively, this is because the attitude kinematics do not encode any information about the relative velocity and wind states. They only depend on the measured angular velocity. Therefore, introducing terms in the relative velocity and wind observer dynamics that depend on the attitude estimate error only degrades observer performance. The matrix $\boldsymbol{L}_1$ is left as a free tuning parameter. It can be chosen using similar methods to that of a Kalman filter or other Luenberger observer. Altogether, the matrix $\boldsymbol{L}$ is given in Eq. (54).

$$\boldsymbol{L} = \begin{bmatrix} \boldsymbol{L}_{1_q} & \boldsymbol{0} & \boldsymbol{0} & \boldsymbol{0} \\ \boldsymbol{0} & \boldsymbol{L}_{1_\lambda} & \boldsymbol{0} & \boldsymbol{0} \\ \boldsymbol{0} & \boldsymbol{0} & \boldsymbol{L}_{1_\zeta} & \boldsymbol{0} \\ \boldsymbol{0} & \boldsymbol{0} & \boldsymbol{0} & \boldsymbol{L}_{1_\omega} \\ \boldsymbol{\Gamma}_{v,q}\boldsymbol{R}_{\mathrm{IB}}^\top \boldsymbol{L}_{1_q} & \boldsymbol{0} & \boldsymbol{0} & \boldsymbol{\Gamma}_{v,\omega}\boldsymbol{M}_v^\top \boldsymbol{I}\boldsymbol{L}_{1_\omega} \\ \boldsymbol{R}_{\mathrm{IB}}\boldsymbol{\Gamma}_{w,q}\boldsymbol{R}_{\mathrm{IB}}^\top \boldsymbol{L}_{1_q} & \boldsymbol{0} & \boldsymbol{0} & \boldsymbol{R}_{\mathrm{IB}}\boldsymbol{\Gamma}_{w,\omega}\boldsymbol{M}_v^\top \boldsymbol{I}\boldsymbol{L}_{1_\omega} \end{bmatrix} \quad (54)$$

Thus we arrive at the main result of this paper, which is a direct result of Theorem 1.

**Theorem 2.** *Consider the aircraft in wind described by Eq. (18) and the observer in Eq. (21) with $\boldsymbol{L}$ given by Eq. (54). Suppose there exists a positive constant $\gamma$ such that LMI conditions Eq. (43) and Eq. (45) hold. Then the feedback in Eq. (27) with $\varphi_1$ and $\varphi_2$ given by Eq. (52) globally renders the augmented system strictly passive with respect to $\mathcal{M}$. Upon setting $\boldsymbol{v}_d = \boldsymbol{0}$, $\mathcal{M}$ is rendered positively invariant and globally asymptotically attractive.*

## 5 Simulation Results

The designed observer was implemented using simulated flight data of a small fixed-wing UAS called the My Twin Dream, shown in Figure 2. A nonlinear

Figure 2: My Twin Dream Research Aircraft

aerodynamic model was developed for this aircraft in [28] which was linearized about a nominal flight condition to obtain the matrices $\boldsymbol{F}_{(\cdot)}$ and $\boldsymbol{M}_{(\cdot)}$. Then, this model was simulated in MATLAB using large-amplitude open loop controls to excite the nonlinear dynamics. The aircraft was simulated in a uniform wind field with components $W_N = 10$, $W_E = -15$, and $W_D = -3$, as seen in Figure 3. Then, the nonlinear passivity-based observer was implemented on this data. Two violations to the assumptions of the observer design were considered. First, measurement noise was added indicative of typical estimate error from a low-level filter that obtains $\boldsymbol{x}_1$. Then, the aerodynamic matrices $\boldsymbol{F}_v$ and $\boldsymbol{M}_v$ were perturbed randomly to test the observer's robustness to aerodynamic modeling error.

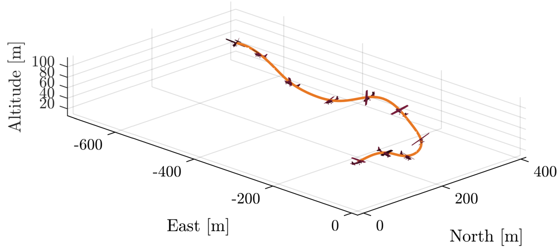


Figure 3: Simulated aircraft trajectory in wind

First the observer was simulated with all assumptions satisfied. That is, the model is perfectly known, there is no measurement noise, and the wind is constant. The convex optimization problem stated in Eq. (47) was solved with $\gamma = 1.54$. The wind estimate results are shown in Figure 4. The observer shows good convergence even with high wind speeds for a small UAS. The bounding functions were also plotted and are shown in Figure 5 where the nonlinear nature of the observer injection is evident.

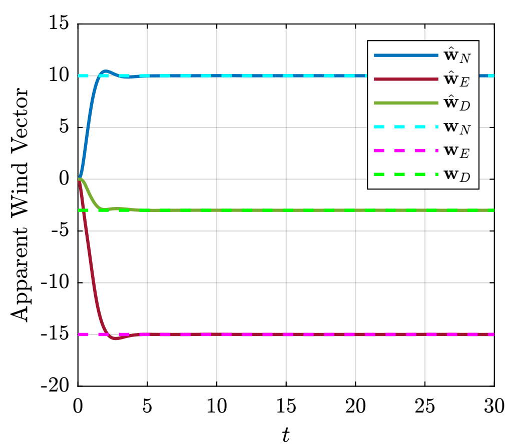


Figure 4: Passivity-based wind estimates

Then, Gaussian measurement noise was added with standard deviations of $\sigma_q = 0.1$, $\sigma_\lambda = 0.05$, $\sigma_\zeta = 0.01$, and $\sigma_\omega = 0.001$ for position, compass vector, tilt vector, and angular velocity, respectively. While the observer somewhat amplifies this noise, the results as shown in Figure 6 still show good performance even with a violation of Assumption 4.

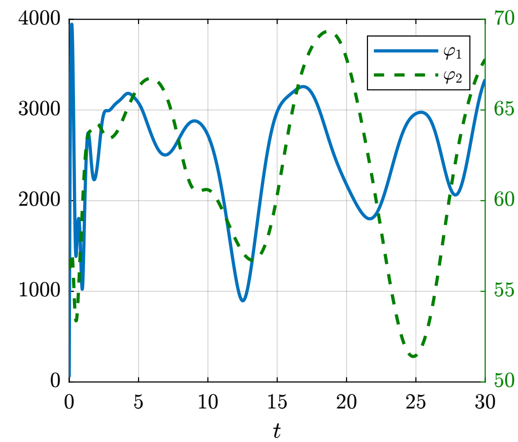


Figure 5: Bounding functions $\varphi_1$ and $\varphi_2$

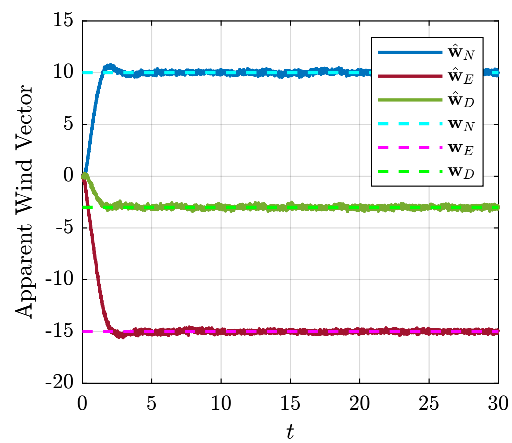


Figure 6: Wind estimates with measurement noise

Finally, the aerodynamic model used to design and implement the observer was randomly perturbed in addition to the presence of measurement noise. The diagonal elements of the matrices $\boldsymbol{F}_v$ and $\boldsymbol{M}_v$ were arbitrarily perturbed with

$$\hat{\boldsymbol{F}}_v = \boldsymbol{F}_v\left(\mathbb{I} + \mathbf{diag}(\boldsymbol{\nu}_1)\right)$$
$$\hat{\boldsymbol{M}}_v = \boldsymbol{M}_v\left(\mathbb{I} + \mathbf{diag}(\boldsymbol{\nu}_2)\right)$$

where $\boldsymbol{\nu}_1$ and $\boldsymbol{\nu}_2$ are Gaussian random vectors with a standard deviation of 0.25. Then the observer was designed and run using the imperfect values of $\hat{\boldsymbol{F}}_v$ and $\hat{\boldsymbol{M}}_v$. The results are shown in Figure 7, where the wind estimates still converge with good performance.

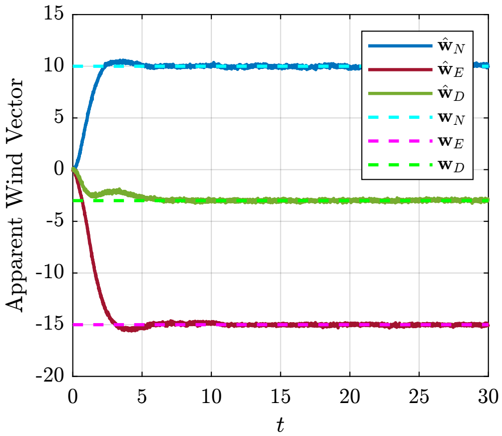


Figure 7: Wind estimates with measurement noise and a perturbed aerodynamic model

## 6 Conclusions and Future Work

This paper details the design and simulation of a global nonlinear passivity-based wind observer for aircraft. Under some reasonable assumptions about the wind field and time scale of the aircraft's aerodynamics, we obtain rigorous guarantees about the convergence of wind estimates across the entire flight envelope. Such strong results help expand the range of flight conditions for which accurate wind estimates can be made. Through a clever choice of injection gain function $\boldsymbol{L}_2$, a linear matrix inequality result was developed that proves the observer error dynamics are globally minimum phase. Then, explicit formulas for the bounding functions that define the scalar injection $k$ were derived. The result of Theorem 2 is generally applicable to a wide variety of aircraft, providing a powerful capability to estimate wind with rigorous guarantees even in adverse conditions. Future work involves implementing this observer on flight test data from both multirotor and fixed wing air vehicles as well as relaxing the assumption of linear, quasi-steady aerodynamics.

## Acknowledgments

The authors gratefully acknowledge the support of the Virginia Space Grant Consortium under the graduate research fellowship. The authors thank Mekonen Halefom, Kenneth Gahan, and Zakia Ahmed for their continually fruitful discussions on wind estimation.

## References

[1] C. Reiche, A. P. Cohen, and C. Fernando, "An Initial Assessment of the Potential Weather Barriers of Urban Air Mobility," *IEEE Transactions on Intelligent Transportation Systems*, vol. 22, pp. 6018–6027, Sept. 2021.

[2] "NASA Aeronautics Strategic Implementation Plan 2019 Update," tech. rep., National Aeronautics and Space Administration, 2019.

[3] B. Hill, D. DeCarme, M. Metcalfe, C. Griffin, S. Wiggins, C. Metts, B. Bastedo, M. Patterson, and N. Mendonca, "UAM Vision Concept of Operations," tech. rep., National Aeronautics and Space Administration, 2020.

[4] M. Patterson, D. Isaacson, and N. Mendonca, "Intermediate State UAM Vision Concept of Operations (ConOps) Overview," Feb. 2021.

[5] D. A. Karr, D. J. Wing, T. L. Barney, V. Sharma, T. J. Etherington, and J. L. Sturdy, "Initial Design Guidelines for Onboard Automation of Flight Path Management," in *AIAA AVIATION Forum*, (VIRTUAL EVENT), July 2021.

[6] D. P. Thipphavong, R. Apaza, B. Barmore, V. Battiste, B. Burian, Q. Dao, M. Feary, S. Go, K. H. Goodrich, J. Homola, H. R. Idris, P. H. Kopardekar, J. B. Lachter, N. A. Neogi, H. K. Ng, R. M. Oseguera-Lohr, M. D. Patterson, and S. A. Verma, "Urban Air Mobility Airspace Integration Concepts and Considerations," in *2018 Aviation Technology, Integration, and Operations Conference*, (Atlanta, Georgia), American Institute of Aeronautics and Astronautics, June 2018.

[7] J. González-Rocha, C. A. Woolsey, C. Sultan, and S. F. J. De Wekker, "Sensing Wind from Quadrotor Motion," *Journal of Guidance, Control, and Dynamics*, vol. 42, pp. 836–852, Apr. 2019.

[8] J. Jacob, P. Chilson, A. Houston, and S. Smith, "Considerations for Atmospheric Measurements with Small Unmanned Aircraft Systems," *Atmosphere*, vol. 9, p. 252, July 2018.

[9] B. Witte, R. Singler, and S. Bailey, "Development of an Unmanned Aerial Vehicle for the Measurement of Turbulence in the Atmospheric Boundary Layer," *Atmosphere*, vol. 8, p. 195, Oct. 2017.

[10] R. T. Palomaki, N. T. Rose, M. van den Bossche, T. J. Sherman, and S. F. J. De Wekker, "Wind Estimation in the Lower Atmosphere Using Multirotor Aircraft," *Journal of Atmospheric and*

*Oceanic Technology*, vol. 34, pp. 1183–1191, May 2017.

[11] J. W. Langelaan, N. Alley, and J. Neidhoefer, "Wind Field Estimation for Small Unmanned Aerial Vehicles," *Journal of Guidance, Control, and Dynamics*, vol. 34, pp. 1016–1030, July 2011.

[12] K. A. Adkins, M. Akbas, and M. Compere, "Real-Time Urban Weather Observations for Urban Air Mobility," *International Journal of Aviation, Aeronautics, and Aerospace*, vol. 7, no. 4, 2020.

[13] R. Trub, D. Moser, M. Schafer, R. Pinheiro, and V. Lenders, "Monitoring Meteorological Parameters with Crowdsourced Air Traffic Control Data," in *2018 17th ACM/IEEE International Conference on Information Processing in Sensor Networks (IPSN)*, (Porto), pp. 25–36, IEEE, Apr. 2018.

[14] H. Shim, J. H. Seo, and A. R. Teel, "Nonlinear observer design via passivation of error dynamics," *Automatica*, vol. 39, pp. 885–892, May 2003.

[15] H. Shim, *A Passivity-based Nonlinear Observer and a Semi-global Separation Principle*. Ph.D. Dissertation, School of Electrical Engineering, Seoul National University, Feb. 2000.

[16] C. Woolsey and L. Techy, "Cross-track control of a slender, underactuated AUV using potential shaping," *Ocean Engineering*, vol. 36, pp. 82–91, Jan. 2009.

[17] T. Battista, S. Jung, C. Woolsey, and E. Paterson, "An energy-casimir approach to underwater vehicle depth and heading regulation in short crested waves," in *2017 IEEE Conference on Control Technology and Applications (CCTA)*, (Mauna Lani Resort, HI, USA), pp. 217–222, IEEE, Aug. 2017.

[18] J.-M. Fahmi and C. A. Woolsey, "Port-Hamiltonian Flight Control of a Fixed-Wing Aircraft," *IEEE Transactions on Control Systems Technology*, vol. 30, pp. 408–415, Jan. 2022.

[19] J.-M. Fahmi and C. A. Woolsey, "Passivity Based Cross-Track Control of a Fixed-Wing Aircraft," in *Conference on Guidance, Navigation and Control*, May 2022.

[20] B. Etkin, "Turbulent Wind and Its Effect on Flight," *Journal of Aircraft*, vol. 18, pp. 327–345, May 1981.

[21] C. I. Byrnes, A. Isidori, and J. C. Willems, "Passivity, feedback equivalence, and the global stabilization of minimum phase nonlinear systems," *IEEE Transactions on Automatic Control*, vol. 36, pp. 1228–1240, Nov. 1991.

[22] Jiang, Zhong-Ping and D. J. Hill, "Passivity and disturbance attenuation via output feedback for uncertain nonlinear systems," *IEEE Transactions on Automatic Control*, vol. 43, pp. 992–997, July 1998.

[23] A. Venkatraman and A. van der Schaft, "Full-order observer design for a class of port-Hamiltonian systems," *Automatica*, vol. 46, pp. 555–561, Mar. 2010.

[24] Y.-C. Chen and C. Woolsey, "Passivity-Based Disturbance Observer Design," (Virtual, Online), p. V001T21A007, American Society of Mechanical Engineers, Oct. 2020.

[25] Y.-C. Chen and C. A. Woolsey, "Nonlinear, Model-Based Disturbance Estimation for Fixed-Wing Aircraft," in *AIAA Scitech 2021 Forum*, (VIRTUAL EVENT), American Institute of Aeronautics and Astronautics, Jan. 2021.

[26] H. K. Khalil, "Chapter 14: Nonlinear Design Tools," in *Nonlinear Systems*, pp. 551–646, Upper Saddle Ridge, New Jersey: Prentice Hall, 3rd ed., 2002.

[27] J. W. Hopwood and C. A. Woolsey, "Passivity-Based Wind Estimation Using Aircraft," *In preparation*, 2023.

[28] J. L. Gresham, B. M. Simmons, J.-M. W. Fahmi, and C. A. Woolsey, "Remote Uncorrelated Pilot Inputs for Nonlinear Aerodynamic Model Identification from Flight Data," in *AIAA AVIATION 2021 FORUM*, (VIRTUAL EVENT), American Institute of Aeronautics and Astronautics, Aug. 2021.